Cement and Concrete Research 142 (2021) 106345

Contents lists available at ScienceDirect

Cement and Concrete Research

journal homepage: www.elsevier.com/locate/cemconres

Quantitative assessment of the influence of external magnetic field on clustering of nano-Fe_3O_4 particles in cementitious paste

Dengwu Jiao [a,b], Karel Lesage [a], Mert Yucel Yardimci [a], Khadija EL CHEIKH [a], Caijun Shi [b], Geert De Schutter [a,*]

[a] Magnel-Vandepitte Laboratory, Department of Structural Engineering and Building Materials, Ghent University, 9052 Ghent, Belgium
[b] Key Laboratory for Green and Advanced Civil Engineering Materials and Application Technology of Hunan Province, College of Civil Engineering, Hunan University, Changsha 410082, China

ARTICLE INFO

Keywords:
Active rheology control (ARC)
Cement paste
Fe-element distribution
Magnetic field
Nano-Fe_3O_4 particles

ABSTRACT

In view of active rheology control of cementitious materials, nano-Fe_3O_4 can be added as responsive particles. Following the concept of magnetorheological fluids, it is assumed that magnetic nanoparticles will form chains or clusters in cementitious paste following magnetic field lines. A quantitative experimental validation of this assumption is presented herein. The clustering of nano-Fe_3O_4 particles under magnetic fields is studied by mapping iron (Fe) element distribution in cementitious paste using energy dispersive X-ray spectroscopy. By means of image analysis, the Fe-element patterns are quantified by the deviation of Fe-elements in a unit area from the mean value expected in case of a uniform distribution, as expressed by coefficient of variation (COV). The magneto-rheological responses of cementitious pastes are evaluated using small amplitude oscillatory shear technique. Results show that the magneto-rheological effect exhibits a linear relationship with the relative change of COV, providing a quantitative validation of magnetic clustering in cementitious paste.

1. Introduction

Pumping is a convenient approach for processing of fresh concrete, especially in large-scale and high-rise projects. Multiple properties of fresh concrete, such as yield stress, viscosity, air content and even temperature, change with the pumping process [1,2]. The aforementioned changes induced by pumping are inevitable and hardly controllable. That is, once the mixture proportion is fixed, the fresh concrete will be pumped according to its initial mixture-dependent properties, which cannot be controlled in real time during the pumping process. In this case, concrete mixtures with appropriate flowability, moderate thixotropy and excellent stability are desired. Specially, when a short interruption is experienced in pumping process, e.g. delay of concrete truck, resuming pumping can be jeopardized if the concrete is highly thixotropic [3]. By contrast, after casting concrete into formwork, mixtures with high thixotropic structural build-up have a potential to reduce formwork pressure and speed up construction process [4–6]. This means that the requirement in the thixotropic structural build-up is contradictious for pumping and formwork casting. Contradicting requirements in properties also exist in 3D concrete printing [7,8]. Accordingly, an advanced construction technique is required to satisfy future challenges.

"SmartCast" [7,9] is a ground-breaking concept aiming at active rheology control (ARC) and active stiffening control (ASC) of cementitious materials. The thixotropic structural build-up of fresh concrete with responsive particles can be artificially controlled by activating an external trigger signal [9], in order to optimize concrete pumping, casting and 3D printing operations. The term "control" is commonly used in adjusting the properties of cement-based materials. For example, Meng and Khayat [10] proposed a method to improve flexural strength of ultra-high performance concrete (UHPC) by controlling the plastic viscosity of suspending mortar with viscosity modified admixture (VMA). Jones et al. [11] demonstrated that hydration and rheology control could be achieved by using limestone powder to meet the requirements of 3D printing. Most of the current property control methods in cement-based materials rely on pre-adding additives or chemical admixtures to obtain desired properties, according to the relationships between properties and mixture proportions [12–14]. The properties of prepared concrete mixtures, however, cannot be further controlled during casting processes. Active control, as considered in "SmartCast", is

* Corresponding author.
E-mail address: Geert.DeSchutter@UGent.be (G. De Schutter).

https://doi.org/10.1016/j.cemconres.2020.106345
Received 17 March 2020; Received in revised form 23 June 2020; Accepted 17 December 2020
Available online 13 January 2021

an essential way to advance construction technology and make pumping, casting and 3D printing processes more reliable.

A potential approach to achieve active rheological control is adding magnetic particles in combination with exploiting magnetic field [7,15–17]. From the standpoint of magnetic particles, ferroferric oxide (Fe_3O_4 or Magnetite) nanoparticles have attracted extensive attention in cement-based materials. Indeed, there are several benefits to the properties of cementitious materials containing nano-Fe_3O_4 particles. Contrary to the most popular nanoparticles (such as nanosilica and nanoclay), the addition of nano-Fe_3O_4 particles with large particle size (such as 50–100 nm) showed less influence on workability of fresh mortars possibly due to their non-porous morphology and hydrophobic characteristics [18]. The usage of nano-magnetite particles has no significant effect on the chemical hydration as well as the main hydration products [19], except for the formation of calcium iron hydroxide silicate with reasonable hydraulic character [20]. Most importantly, cement-based materials containing nano-Fe_3O_4 particles generally exhibit increased mechanical properties due to their nucleation effect and nano-filling effect [18]. Furthermore, the electrochemical stability, electromagnetic wave absorption properties, and the resistance to water absorption and chloride penetration of cementitious materials can be enhanced dramatically with the incorporation of nano-Fe_3O_4 particles [21–23].

Magnetic or electromagnetic fields have been previously applied to cement-based materials, e.g. aligning steel fibers [24,25], improving concrete pumpability [26] and adjusting rheological properties [15–17]. A review can be found in [9]. The controllable rheology of cementitious pastes by applying magnetic field is based on the theoretical foundations of magnetorheological (MR) fluids. For conventional MR fluids consisting of magnetic particles in a Newtonian fluid carrier, magnetic chains and/or columns can be easily observed [27–29]. However, the formation of clusters or columnar structures of magnetic nanoparticles in cement-based suspensions is still unclear due to the resistance induced by the viscoelastic properties of the suspension. Further research on qualitatively and quantitatively assessing magnetic structures in cement-based suspensions is required.

In the current study, the influence of external magnetic field on clustering of nano-Fe_3O_4 particles in cementitious paste is quantitatively evaluated by mapping Fe-element distribution using energy dispersive X-ray (EDX) spectroscopy. Several cementitious paste mixtures, considering the influence of magnetic field strength, nano-Fe_3O_4 particles content and paste medium, are prepared. The rheological properties of the fresh pastes under zero magnetic field as well as the magneto-rheological response are first experimentally investigated by means of flow curve test and small amplitude oscillatory shear technique, respectively. The EDX elemental mapping of Fe is quantitatively converted into the distribution of Fe-element number by using image analysis technique. The effects of magnetic field strength, nanoparticles content and paste medium on the Fe-element quantitative distribution are discussed in combination with the magneto-rheological response. The relationship between the magneto-rheological properties and Fe-element quantitative distribution is established.

2. Experimental program

2.1. Materials

Ordinary Portland cement (OPC) CEM I 42.5 N conforming to EN 196-1 [30] is utilized in this study. The chemical composition and particle size distribution are shown in Table 1 and Fig. 1, respectively. The specific gravity and specific surface area (Blaine) of the Portland cement are 3.15 and 279.5 m^2/kg, respectively. Spherical Iron Oxide nano-Fe_3O_4 particles (MNPs) with Fe_3O_4 purity higher than 98% (from US Research Nanomaterials, Inc) are used. The average particle size, specific surface area and relative density of the nano-Fe_3O_4 particles supplied from the manufacture are 20–30 nm, 40–60 m^2/g and 4.95, respectively. To determine the magnetic properties of the cement and nanoparticles, the curves of magnetization versus magnetic field strength were obtained from a vibrating sample magnetometer, as shown in Fig. 2. Under an external magnetic field, the magnetic domains in magnetic materials align parallel to the direction of the magnetic field, creating a magnetic dipole moment, i.e. magnetization. At sufficiently high magnetic field, the magnetization remains nearly constant and this value is defined as saturation magnetization (*Ms*). It can be observed from Fig. 2 that the *Ms* of the cement and nano-Fe_3O_4 particles is about 0.59 emu/g and 49.48 emu/g, respectively. A commercial polycarboxylate ether superplasticizer (PCE) (MasterGlenium 51) is employed. All samples are prepared using de-ionized water.

Table 1
Chemical composition of the Portland cement.

Components	% by mass
SiO_2	19.6
Al_2O_3	4.88
Fe_2O_3	3.14
CaO	63.2
MgO	1.8
SO_3	2.9

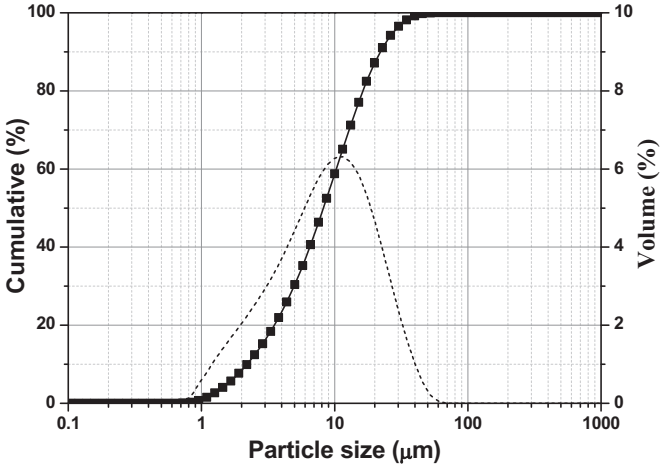

Fig. 1. Particle size distribution of the Portland cement.

2.2. Mixing procedure

Several batches of cementitious pastes were selected by considering the influences of nano-Fe_3O_4 particles content (1% and 3% by mass of cement paste (cement + water)), paste medium (w/c = 0.4, w/c = 0.35, w/c = 0.35 + 0.6%PCE) and magnetic field strength (0 T, 0.25 T, 0.5 T, 0.75 T). A mass of 20 g of cement was used for each sample. The mixture proportions of the cementitious pastes and the selected magnetic fields are listed in Table 2. The cementitious paste was mixed using a rotational rheometer (MCR 52, Anton Paar) with a helix geometry. Prior to

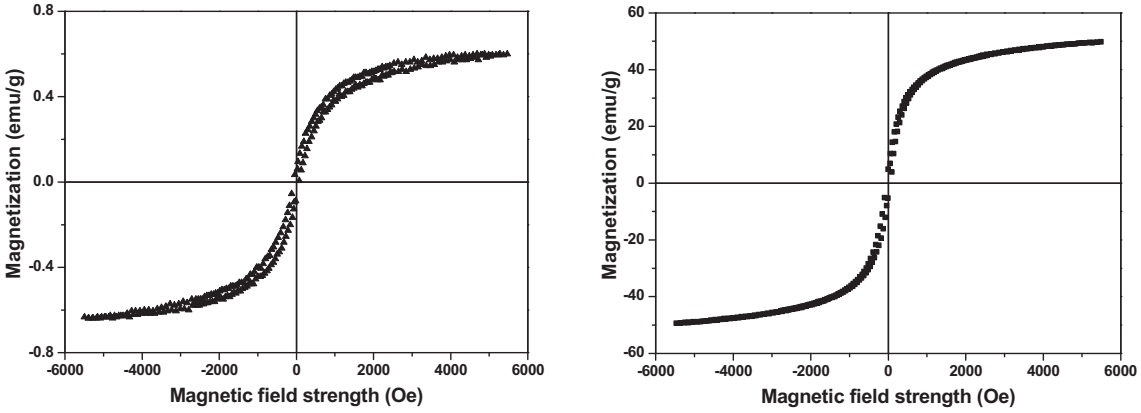

Fig. 2. Magnetization versus magnetic field strength curves (1 T = 10,000 Oe).

Table 2
Mixture proportions of cementitious pastes and the applied magnetic fields.

No.	Cement (g)	Water (g)	MNPs (g)	PCE (g)	Magnetic field
0.4_R	20	8	0	0	0 T, 0.5 T
0.4_3%MNPs	20	8	0.84	0	0 T, 0.25 T, 0.5 T, 0.75 T
0.4_1%MNPs	20	8	0.28	0	0 T, 0.5 T
0.35_3%MNPs	20	7	0.81	0	0 T, 0.5 T
0.35_0.6% PCE_3%MNPs	20	7	0.81	0.12	0 T, 0.5 T

introduction, the nanoparticles have not been specially treated in view of improving dispersion. The high shear mixing with rotational speed of 3000 r/min provides a repeatable initial state of paste samples. The details of the geometric parameters of the helix geometry and the mixing procedure can be found in [15].

2.3. Testing methods

2.3.1. Flow curve test

The flow curve test was conducted to assess the rheological properties of the cementitious pastes in the absence of an external magnetic field. A rotational parallel plate rheometer (MCR 102, Anton Paar) with magneto-rheological device (MRD) was used. A uniform magnetic field perpendicular to the plates can be applied to the sample by inputting specific current. The diameter of the upper plate is 20 mm and the gap between the upper and lower plates is fixed at 1 mm. After pouring the sample into the plate of the rheometer, a pre-shearing with shear rate of 100 s^{-1} was first applied for 30 s. Afterwards, the shear rate logarithmically decreased from 100 s^{-1} to 0.1 s^{-1} within 100 s, and the points of shear stress versus shear rate were recorded every second. During the flow curve test, the temperature of all samples was controlled at 20 ± 0.5 °C.

2.3.2. Determination of magneto-rheological effect

The strain sweep test with strain amplitude from 0.0001% to 10% and constant frequency of 2 Hz was first conducted to determine the linear viscoelastic region (LVER). The critical strain of all the studied cementitious pastes was around 0.01% or even higher. Therefore, the strain amplitude in oscillatory time sweep test for evaluating the response of the cementitious pastes to an external magnetic field was selected as 0.001%. The sample in the plate of the rheometer was first per-sheared at shear rate of 100 s^{-1} for 30 s and then rested for 10 s. This was followed by the oscillatory time sweep test with constant strain amplitude and frequency of 0.001% and 2 Hz [15], respectively. The magnetic field was applied to the sample at the beginning of the time sweep test according to the selected field strength in Table 2. The temperature of all the samples was fixed at 20±0.5 °C during the time sweep test. It should be mentioned here that the flow curve test and time sweep test were performed separately using fresh samples, and for each mixture proportion, three rheological reproducible tests on three alternative samples were conducted. A representative oscillatory time sweep test result for Mix. 0.4_3%MNPs is plotted in Fig. 3. It can be seen that the cementitious paste showed distinct evolution in storage modulus under 0 T and 0.5 T. For simplicity and comparison, the storage modulus at magnetization of 300 s ($G'_{t=300s}$) was utilized as a parameter to describe the rheological response of the cementitious paste to an external magnetic field, and the magneto-rheological effect can be expressed by the relative change of $G'_{t=300s}$. Here, for instance, the magneto-rheological effect of the Mix. 0.4_3%MNPs responding to the magnetic field of 0.5 T can be expressed as:

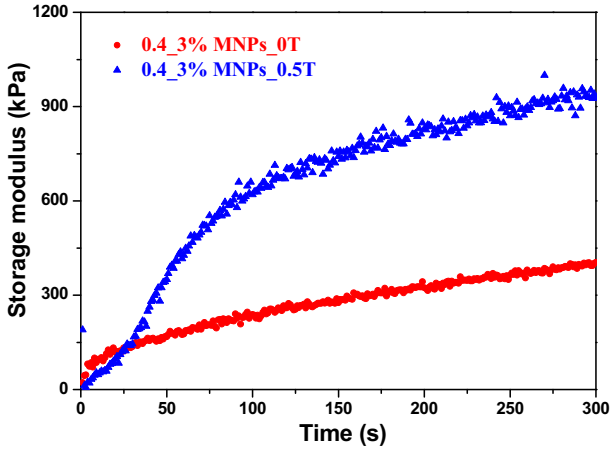

Fig. 3. Representative oscillatory time sweep testing result of Mix. 0.4_3%MNPs.

$$R_{G'_{t=300s}} = \frac{G'_{t=300s}(0.5\mathrm{T}) - G'_{t=300s}(0T)}{G'_{t=300s}(0T)} \times 100\% \quad (1)$$

where $G'_{t=300s}$(0 T) and $G'_{t=300s}$(0.5 T) are the storage modulus at 300 s under the magnetic field of 0 T and 0.5 T, respectively. Larger $R_{G't=300s}$ indicates higher magneto-rheological effect.

2.3.3. Scanning electron microscopy (SEM) test

After preparing the sample according to the method described in

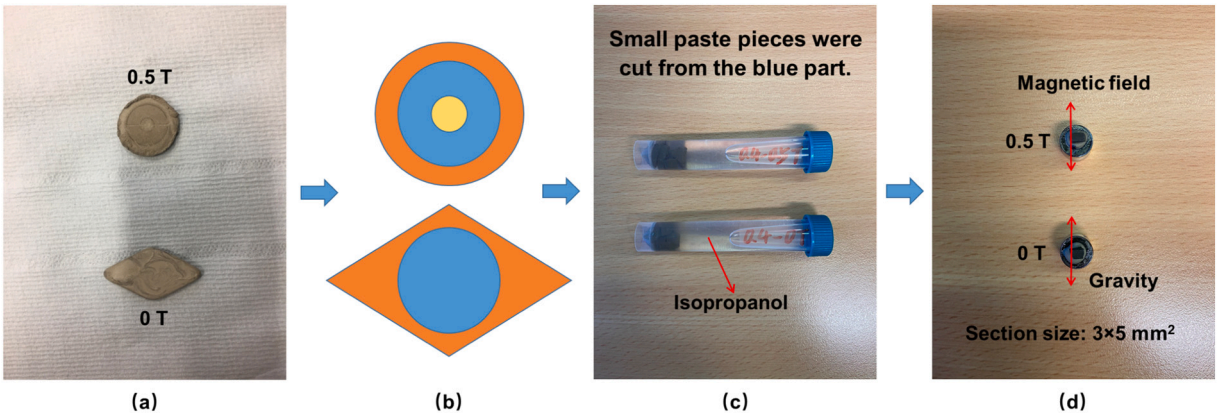

Fig. 4. Main processes of sample preparation for the SEM test.

Section 2.2, part of the cementitious paste was poured into the plate of the rheometer with specific magnetic field as illustrated in Table 2. To ensure the samples with and without magnetic field have similar initial microstructure, on the other hand, a plastic mold was used to pour the rest paste in the absence of magnetic field. After 12 h, the magnetic field was removed, and both paste discs with thickness of approx. 3 mm, as shown in Fig. 4 (a), were cured at a chamber with temperature of 25 °C and humidity of 50 ± 5% for 2.5 days. Afterwards, small paste pieces with cross section size of approx. 3 mm × 5 mm were cut by hand from the blue part in Fig. 4 (b) and kept in isopropanol for 7 days to stop the chemical hydration. This is followed by putting the pieces in a vacuum desiccator until SEM test. Before the SEM test, the samples were dried in an oven with 40 °C for 3 days to remove the isopropanol. Then one or two pieces for each mixture were randomly chosen to perform the SEM measurement, as shown in Fig. 4 (d). The morphology and elemental mapping of Fe on the original cross section parallel to the direction of the magnetic field (and gravity for the discs without magnetic field) were obtained by using a SEM device (QUANTA FEG250) employing energy dispersive X-ray spectroscopy. All images were acquired at magnification of 1000×. A total of 101 elemental maps of Fe were taken, so that for each situation mentioned in Table 2, an average 8 images has been obtained, yielding representative information. Through image processing, the Fe-element distribution on the cross section can be quantified, which gives an indication of the clustering of nano-Fe_3O_4 particles in cementitious paste.

2.3.4. *Fe-element distribution analysis*

Fig. 5 shows the image analysis process for the quantification of the Fe-element distribution in the cross section parallel to the direction of the magnetic field (or gravity). The EDX elemental maps of Fe (called RGB images) with resolution of 1024 × 896 pixels were first converted into binary images by using MATLAB software. The actual size of 1 pixel is 0.293 μm. The white pixel in the binary images represents the Fe-element, and the black pixel means the surrounding matrix. Therefore, the detailed information of Fe-element points in the cross section, such as number and proportion, can be obtained by analyzing the binary images. To evaluate the Fe-element distribution, each binary image was divided equally into 12 × 11 units composed of 80 × 80 pixels, resulting in a modified binary image with resolution of 960 × 880 pixels. The remaining pixels of the original 1024 × 896 image, located in the bottom

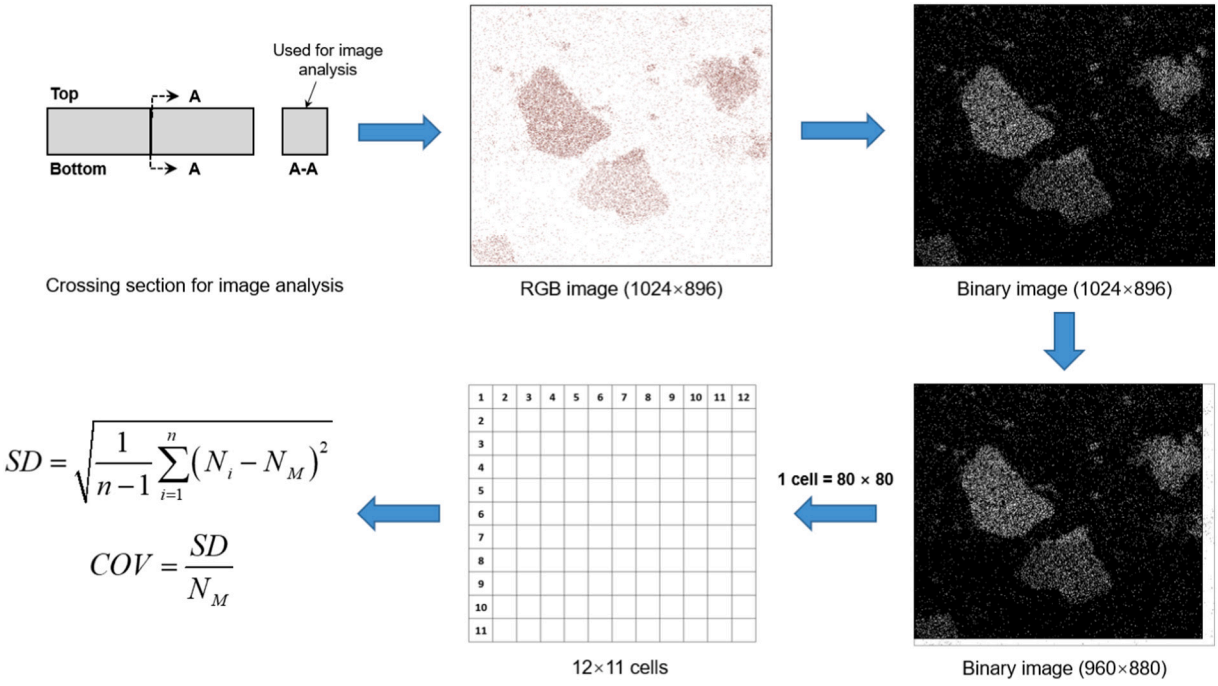

Fig. 5. Image analysis process for the Fe-element distribution in cementitious paste.

and right margins, were discarded. According to the number of Fe-element points in every unit, the standard deviation (*SD*) of the number of Fe-elements for the 132 units can be obtained, as expressed by Eq. (2):

$$SD = \sqrt{\frac{1}{n-1}\sum_{i=1}^{n}(N_i - N_M)^2} \quad (2)$$

where n is the number of units ($n = 132$), N_i is the Fe-element number in i^{th} unit ($i = 1, 2, \ldots, 132$), and N_M is the mean number of Fe-elements in the 132 units. Theoretically, when the Fe-elements are well uniformly distributed within the cross section, the number of Fe-elements should be similar in each unit and the obtained standard deviation should be zero. Higher standard deviation means more agglomerated distribution (i.e. clusters) of Fe-elements on the cross section of the cementitious paste. Given that the total number of identified Fe-elements varies with the image, the coefficient of variation (*COV*) independent of the number is selected to evaluate the Fe-element distribution on the cross section, as described by Eq. (3):

$$COV = \frac{SD}{N_M} \quad (3)$$

The COV expresses the deviation of Fe-elements in a unit area from the mean value. Higher magnitude of COV indicates higher extent of formed clusters of Fe-elements [10,31]. A representative EDX elemental mapping of Fe and the corresponding quantitative analysis results are presented in Fig. 6. It can be seen that the Fe-element patterns can be quantitatively characterized by the number of Fe-elements in the 132 units, and the clustering of Fe-elements can be evaluated by the COV value. The quantitative parameters derived from the 101 EDX elemental maps are summarized in Appendix A.

3. Results and discussion

3.1. Rheological properties of cementitious pastes

The objective of measuring rheological properties is to understand the flow behavior of the cementitious pastes in the absence of an external magnetic field. The curves of shear stress versus shear rate of the studied cementitious pastes are presented in Fig. 7. The cementitious pastes generally exhibited shear thinning behavior at the shear rate region of 1–100 s^{-1}, as the shear viscosity gradually decreased with the increase of shear rate. The addition of nano-Fe_3O_4 particles increased

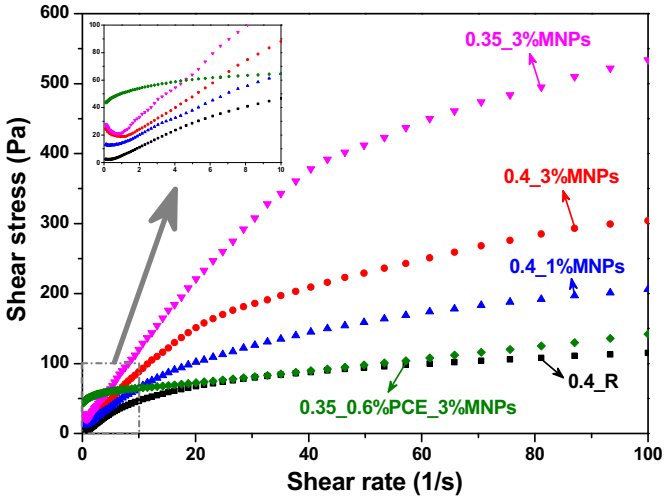

Fig. 7. Flow curves of cementitious pastes under zero magnetic field.

the measured shear stress, indicating a reduction in the flowability of cementitious paste. This is probably due to that the nano-Fe_3O_4 particles with average particle size of 20–30 nm require part of water in the interstitial solution of cement paste to coat their surfaces, thereby reducing the free water in the suspension with lubrication effect. Moreover, the physical nature of the nano-Fe_3O_4 particles with tendency to agglomerate might also be responsible for the increase in stiffness of the cementitious paste [19]. At the same concentration of the nano-Fe_3O_4 particles (i.e. 3%), decreasing w/c of cement paste medium from 0.4 to 0.35 almost doubled the measured shear stress. This means that the reduction effect of nano-Fe_3O_4 particles on the flowability amplified at low w/c. However, the rheological properties of the cementitious paste after adding 0.6% PCE were significantly increased, which had a comparable flowability with the reference cement paste.

The shear stress-shear rate curves of the cementitious pastes showed different trends at relatively low shear rate regions. For the reference cement paste and cementitious paste with 1% nano-Fe_3O_4 particles, the shear stress reduced to a stable value with the decrease of shear rate. By contrast, the cementitious pastes with 3% nano-Fe_3O_4 particles, irrespective of the w/c, the shear stress showed a slightly increasing trend with shear rate decreasing from 1 s^{-1} to 0.1 s^{-1}. This can be explained by the competition between attractive particle interactions and

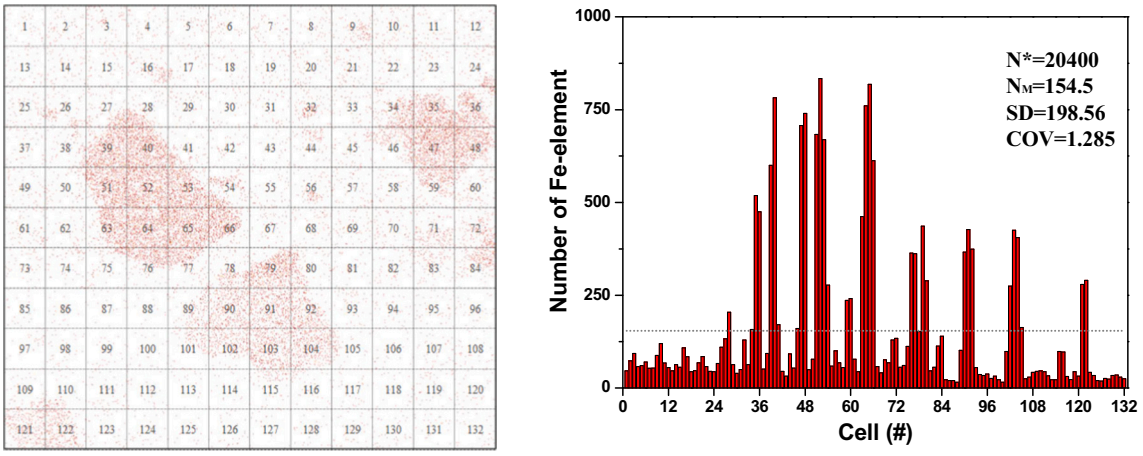

(a) RGB image (960×880) (b) Fe-element distribution

Fig. 6. Representative EDX elemental mapping of Fe and its quantitative analysis results. Note: N* is the total number of Fe-elements identified in each image. N_M is the mean number of Fe-elements in the 132 units. SD and COV are the standard deviation and the coefficient of variation of Fe-elements.

hydrodynamic forces [32,33]. For the cementitious pastes with nano-particles under extremely low shear rates, the attractive forces between solid particles dominate the repulsive and hydrodynamic forces. Small agglomerates and clusters between solid particles, especially nano-Fe_3O_4 magnetic particles, are therefore probably formed, leading to a slightly higher measured shear stress. Besides, the inter-particle contacts might exert a significant resistance to the shear flow with low shear rates. Accordingly, the slightly increasing behavior of shear stress with decreasing shear rate (at low values) can be observed. Most interestingly, the measured shear stress of the cementitious paste with 0.6% PCE and 3% nano-Fe_3O_4 particles decreased continuously in the entire shear rate region, and compared to the other mixtures, it was the highest at low shear rate region (e.g. 0.1–2 s^{-1}). This indicates that under the flow state with low shear rate, the moving cement particles and nanoparticles experienced highest resistance exerted by the suspension.

3.2. Fe-element distribution and magneto-rheological response

3.2.1. Influence of magnetic field strength

Fig. 8 presents the correlations between the coefficient of variation (COV), the storage modulus after magnetization for 300 s ($G'_{t=300s}$) and magnetic field strength. Clearly, for the reference cement paste (0.4_R), the application of an external magnetic field with 0.5 T showed negligible influences on the $G'_{t=300s}$. This indicates that cement paste without additional magnetic particles shows no significant rheological response to the external magnetic field, which is in good agreement with [16]. A representative output Fe-element quantitative distribution is shown in Appendix B (a). It can be seen that non-uniform distributing behavior of Fe-element points in the units can be noticed, as reflected in the non-zero standard deviation (SD) and COV. The identified Fe-element points on the cross section of the reference cement paste come from part of hydration products (such as sulfoferrites of calcium) and unhydrated cement particles. The non-uniform distribution of Fe reveals that the chemical compounds containing Fe-element are not well uniformly distributed in pure cement paste. From Fig. 8 we can see that the calculated COV showed a slightly higher value for the reference cement paste prepared under the external magnetic field of 0.5 T. This result suggests that the iron-containing compounds slightly accumulate, resulting in the formation of small clusters of Fe-elements. This can be attributed to the weak ferromagnetic properties of the Portland cement particles with saturation magnetization of 0.59 emu/g, as presented in Fig. 2 (a). It is worth noting that the slight difference of COV is not in contradiction with the results of storage modulus. The result merely indicates that the imperceptible change in the internal microstructure of the reference cement paste after applying the magnetic field cannot be monitored by using small amplitude oscillatory technique.

For the cementitious paste with 3% nano-Fe_3O_4 (0.4_3%MNPs) prepared in the absence of an external magnetic field, a slightly higher COV than the reference cement paste can be observed. This indicates that there exist small Fe-element clusters on the cross section, which can be explained by the following aspects. The Fe-elements in the Mix. 0.4_3%MNPs are contributed by the Fe in nano-Fe_3O_4 particles and cement particles, regardless of the potential chemical hydration. The Fe-elements from the Portland cement particles are not well uniformly distributed, as mentioned in the above paragraph. After adding the nano-Fe_3O_4 particles, the stiffness of the cementitious paste is increased, showing significant increase in the measured shear stress and $G'_{t=300s}$. The increase of the stiffness and the intrinsic magnetic properties of the nano-Fe_3O_4 have a potential to facilitate the nanoparticles agglomerate to form small clusters. Their synergistic effects provide more chance for the formation of Fe-element clusters. Furthermore, the nano-Fe_3O_4 particles may not be adequately dispersed prior to adding to the cement paste, and the high shear mixing may not be sufficient to properly disperse the nanoparticles. Consequently, the COV of the Mix. 0.4_3% MNPs was slightly higher than that of the pure cement paste.

With the increase of magnetic field strength, the gradual increase of $G'_{t=300s}$ presents a good consistency with the increase of COV. After applying an external magnetic field, the magnetic nano-Fe_3O_4 particles accumulate to form agglomerates and clusters under the magnetic force [34,35]. Due to the viscoelastic properties of the cement-based suspensions, the yield stress and the viscosity of the suspension have a potential to prevent the initial movement and exert a movement resistance to the nano-Fe_3O_4 particles, respectively. The magnetic force between the nano-Fe_3O_4 particles increases with increasing magnetic field strength, and more nano-Fe_3O_4 particles could overcome the local resistance to increase the number of nanoparticles contributing to the clusters. Besides, higher magnetic force results in stronger interactions between the magnetic nanoparticles or clusters. Therefore, in the view of magneto-rheological response, increasing values of $G'_{t=300s}$ with the increase of field strengths were achieved, and from the perspective of Fe-element distribution, gradual increase in COV was recognized. Additionally, the representative figures in Appendix B (c-f) reveal that higher number of clustering Fe-elements obtained with the growth of field strength. If hypothesizing that all the elements are connected, higher magnetic field strength resulted in larger size of Fe-element clusters, displaying the non-uniform behavior more intuitively and easily. The results, in other words, indicate that the increase in COV quantitatively characterizing the non-uniform distribution of Fe-elements provides a sound validation for the hypothesis of the formation and enlargement of magnetic clusters with the increase of magnetic field strength.

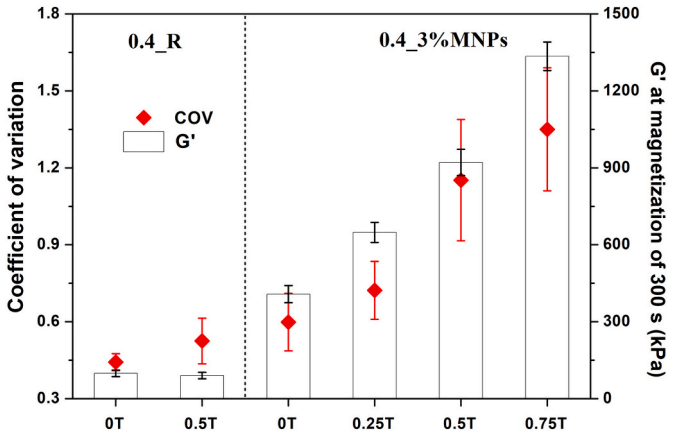

Fig. 8. Effect of magnetic field strength on COV and $G'_{t=300s}$. Error bar indicates the standard deviation.

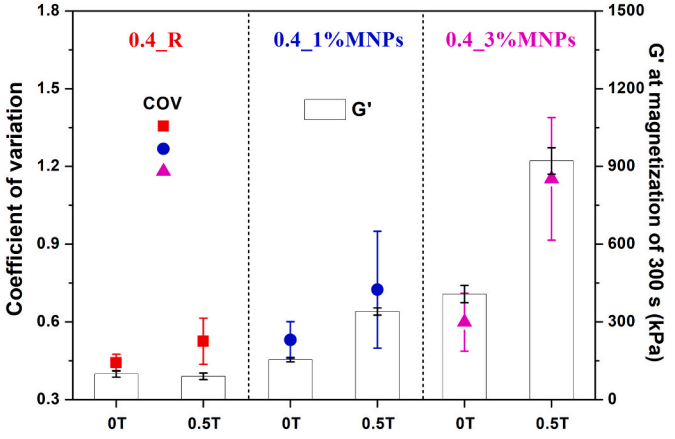

Fig. 9. Influence of nano-Fe_3O_4 contents on COV and $G'_{t=300s}$. Error bar indicates the standard deviation.

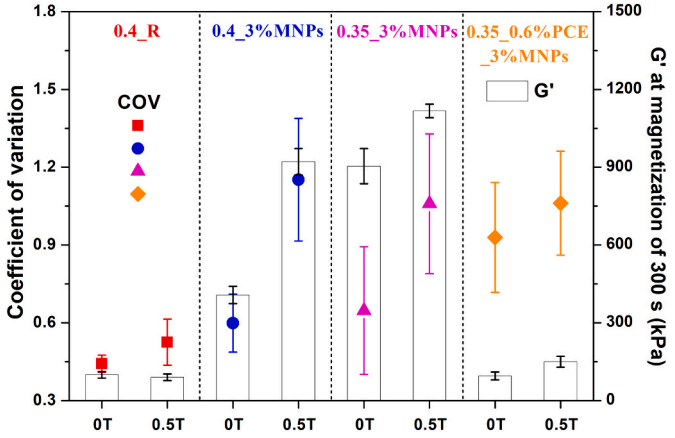

Fig. 10. Effect of cement paste medium on COV and $G'_{t=300s}$. Error bar indicates the standard deviation.

3.2.2. *Influence of nano-Fe_3O_4 content*

The influence of nano-Fe_3O_4 particles content on the COV and $G'_{t=300s}$ is presented in Fig. 9. Without magnetic field, it can be seen that both COV and $G'_{t=300s}$ of the cementitious paste with 1% nano-Fe_3O_4 particles laid in between the values of reference cement paste and cementitious paste with 3% nano-Fe_3O_4 particles. Indeed, comparing with the cementitious paste with 3% nano-Fe_3O_4 particles, the addition of 1% nano-Fe_3O_4 requires less water to coat their surfaces, leaving more free water acting as lubrication. As a result, the cementitious paste with 1% nano-Fe_3O_4 particles only showed a slight increase in the stiffness compared to the reference cement paste. This is in good agreement with the result of COV, which can be attributed to the fact that nanoparticles with lower content are more easily distributed in suspensions with higher flowability. Another possible reason for the low calculated COV of the cementitious paste with 1% nano-Fe_3O_4 is that the low concentration of Fe-elements itself results in more difficult to be identified on the selected cross section.

After applying an external magnetic field of 0.5 T, the cementitious pastes containing nano-Fe_3O_4 particles showed magneto-rheological response, with larger magneto-rheological effect corresponding to higher content of the nanoparticles. According to the hypothesis of magnetic cluster formation, higher particle concentration results in more nanoparticles contributing to the magnetic clusters under the same magnetic field strength. Theoretically, more non-uniform distribution of Fe-elements in the cementitious paste should be obtained with the increase of nanoparticles content, and the degree of non-uniformity of the cementitious paste with 1% nano-Fe_3O_4 should be lower than that of the cementitious paste with 3% nano-Fe_3O_4. Indeed, from the representative figures of Fe-element quantitative distribution in Appendix B (e) and (h), it can be seen that the cementitious paste with lower nanoparticles content exhibited lower number and smaller size of clustering Fe-elements than that with 3% nano-Fe_3O_4 particles under the magnetic field of 0.5 T. It can be observed from Fig. 9 that the COV and the corresponding difference increased with the concentration of nano-Fe_3O_4 particles in the presence of the external magnetic field. The quantitative results of the Fe-element distribution are consistent with the rheological test results and the underlying hypothesis.

3.2.3. *Influence of paste medium*

The influence of paste medium on the COV and $G'_{t=300s}$ is shown in Fig. 10. From the perspective of stiffness, the change of $G'_{t=300s}$ in the absence of the magnetic field is consistent with the measured shear stress, comparing Figs. 7 and 10. Reducing w/c of the paste medium from 0.4 to 0.35 decreased the difference of $G'_{t=300s}$ between 0.5 T and 0 T. That is, cementitious paste with lower water content and higher solid concentration generally exhibits lower magneto-rheological effect. This can be explained by the high stiffness of the suspensions [36]. After adding 0.6% PCE into the cementitious paste with 3% nano-Fe_3O_4 particles (Mix. 0.35_0.6%PCE_3%MNPs), the cementitious paste under zero magnetic field showed a comparable $G'_{t=300s}$ to the reference cement paste, but the magneto-rheological effect was far less than that of Mix. 0.4_3%MNPs. The mixture of 0.35_0.6%PCE_3%MNPs possessed relatively high shear stress at low shear rates, as presented in Fig. 7, exerting high resistance to the movement of nanoparticles to form magnetic clusters. This means that only some limited nanoparticles clusters may be formed. From the viewpoint of G', the mixture showed a weak stiffness, as shown in Fig. 10. In this case, the formation of limited clusters of nanoparticles under the magnetic field of 0.5 T probably cannot significantly increase the stiffness of the suspension, resulting in a slight increase in the $G'_{t=300s}$. Therefore, the Mix. 0.35_0.6%PCE_3%MNPs exhibited a relatively low magneto-rheological effect.

In the view of Fe-element distribution, the value of COV is basically increased for the cementitious pastes prepared under the external magnetic field, regardless of the paste medium. This indicates that the Fe-elements of cementitious paste processed by magnetic field showed more non-uniform distribution than that without magnetic field, which is in good agreement with the response of rheological properties. It is worth mentioning here that the mixture of 0.35_3%MNPs presenting higher stiffness under zero magnetic field still showed higher Fe-element distribution with COV of 0.647. However, for the Mix. 0.35_0.6%PCE_3%MNPs, the COV is around 0.929 under zero magnetic field, in spite of the small $G'_{t=300s}$ and high flowability. This indicates that the addition of PCE increases the fluidity and meanwhile results in more nanoparticles agglomeration in the cementitious paste. The unexpected result probably can be explained by the interaction between nano-Fe_3O_4 particles and PCE. Nanoparticles in cement-based materials generally play their role as agglomerates with grain size in submicron, even in well-dispersed suspensions [37]. The effect of nanoparticles on flowability depends on the size of agglomerates [38]. Although the nanoparticles can require more water due to the high specific surface area, the small agglomerates could fill the voids between cement particles, releasing free water and improving flowability of the suspension. However, the large agglomerates absorb free water with lubricating effect and then decrease the flowability. In the case of the current research, on the one hand, the addition of 0.6% PCE improves the dispersion of cement particles, exhibiting a significant increase in the flowability and reduction in the stiffness. On the other hand, the plasticizing effect of the PCE possibly has no apparent effect on the dispersion of the nano-Fe_3O_4 particles, as can be observed from the COV values of 0.35_3%MNPs_0.5 T and 0.35_0.6%PCE_3%MNPs_0.5 T. Consequently, small agglomerates of nano-Fe_3O_4 exist in the voids between the well dispersed cement particles, and thus non-uniform distribution of Fe-elements is observed from the EDX elemental mapping. The many small clustering Fe-elements in the representative figure in Appendix B (l) provide a reliable evidence for the small agglomerates of nano-Fe_3O_4 particles. Nevertheless, further research is required to study the interactions between nano-Fe_3O_4 particles and PCE in cement-based suspensions.

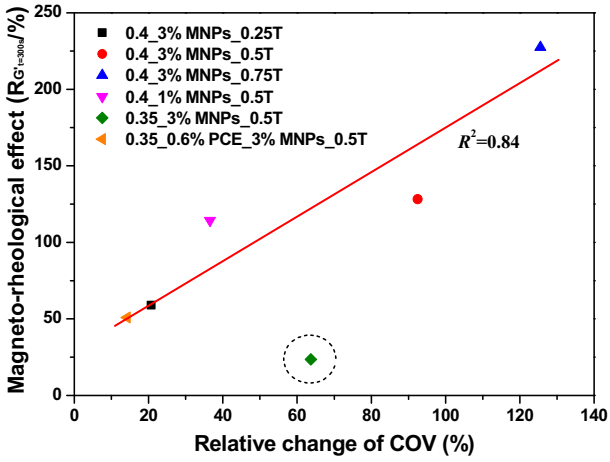

Fig. 11. Relationship between magneto-rheological effect ($R_{G't=300s}$) and relative change of *COV*.

3.3. Correlations between magneto-rheological effect and Fe-element distribution

From the discussion of the quantitative Fe-element distribution and the rheological response to an external magnetic field, it can be easily concluded that the cementitious paste containing nano-Fe_3O_4 particles processed under an external magnetic field generally exhibits more non-uniform distribution of Fe-elements, regardless of the mixture proportion. To correlate the magneto-rheological properties with the Fe-element distribution, the points of relative change of COV (as expressed in Eq. (4)) and the magneto-rheological effect ($R_{G't=300s}$) determined by Eq. (1) are depicted in Fig. 11.

$$R_{COV} = \frac{COV(B) - COV(0T)}{COV(0T)} \times 100\% \quad (4)$$

where *COV*(0 T) is the COV value of the sample under zero magnetic field, and *COV*(*B*) is the value of the sample under specific magnetic field, with magnetic field strength *B* of 0.25 T, 0.5 T or 0.75 T. Although more data is required, it can be seen from Fig. 11 that the magneto-rheological effect shows a linear relationship with the relative change of COV for most of the samples, except the mixture of 0.35_3%MNPs_0.5 T. This result confirms that most of the cementitious pastes containing nano-Fe_3O_4 particles with higher rheological response to an external magnetic field commonly consist of larger and more clusters and agglomerates of Fe-elements. The aberrant point of the Mix. 0.35_3% MNPs_0.5 T might be attributed to the high stiffness of the mixture under zero magnetic field, which can be expressed by the high measured shear stress and the $G'_{t=300s}$(0 T), as presented in Fig. 10. This finding provides an explanation for the increase in stiffness as well as a solid evidence for the formation of magnetic clusters of nano-Fe_3O_4 particles in cementitious paste under an external magnetic field.

4. Conclusions

Cementitious paste containing magnetic nanoparticles shows magneto-rheological behavior. In the present study, the influence of external magnetic field on the clustering of magnetic nanoparticles (nano-Fe_3O_4) in cementitious paste is investigated. The field-induced nanoparticles clustering is correlated with the magneto-rheological properties of the cementitious paste. Based on the obtained results, the following conclusions are reached:

(1) When applying a magnetic field to cementitious paste containing nano-Fe_3O_4 particles, the magnetic nanoparticles tend to cluster, moving away from a fairly uniform distribution in case of absence of the magnetic field.
(2) With the increase of magnetic field strength, the magneto-rheological response is enlarged, as more nano-Fe_3O_4 particles will contribute to the magnetic clusters, increasing the interactions between the magnetic nanoparticles. This is evidenced by an increasing deviation of the distribution of mapped Fe-elements from a uniform spatial distribution, as quantified in coefficient of variation (COV).
(3) The COV derived from the EDX elemental mapping, representative for the spatial clustering of the nano-Fe_3O_4 particles, is a useful quantitative indicator for the magneto-rheological properties of cementitious paste containing magnetic nanoparticles. A linear correlation is found between the magneto-rheological effect and the increase in clustering of nano-Fe_3O_4 particles as quantified with COV.
(4) The obtained results provide a sound experimental validation and quantification of the formation of clusters between magnetic nanoparticles under an external magnetic field as the reason for the stiffness increase of the magneto-rheological cementitious paste.

CRediT authorship contribution statement

Dengwu Jiao: Methodology, Formal analysis, Investigation, Writing – original draft, Visualization. **Karel Lesage:** Conceptualization, Methodology, Resources, Writing – review & editing, Supervision. **Mert Yucel Yardimci:** Writing – review & editing, Supervision. **Khadija E.I. Cheikh:** Writing – review & editing, Supervision. **Caijun Shi:** Writing – review & editing, Supervision. **Geert De Schutter:** Conceptualization, Methodology, Formal analysis, Writing – review & editing, Supervision, Project administration, Funding acquisition.

Declaration of competing interest

The authors declared that we have no conflicts of interest to this work. We declare that we do not have any commercial or associative interest that represents a conflict of interest in connection with the work submitted.

Acknowledgements

This paper is a deliverable of the ERC Advanced Grant project 'SmartCast'. This project has received funding from the European Research Council (ERC) under the European Union's Horizon 2020 research and innovation program (grant agreement No. 693755). The authors gratefully acknowledge the financial support from ERC. Besides, the first author gives special thanks to Qiang Ren for his kind help during the image analysis process.

Appendix A. Summary of the derived parameters from 101 EDX elemental images

Mixture	Image	N*	N_M	SD	COV
0.4_R_0T	1	3317	25.10	11.03	0.44
	2	2525	19.10	8.30	0.43
	3	3097	23.50	11.66	0.50
	4	2007	15.20	6.69	0.44
	5	1944	14.70	5.96	0.40
	Average	2578	19.52	8.73	0.44
	Std. Dev.	622	4.72	2.54	0.03
0.4_R_0.5 T	1	2315	17.50	8.81	0.50
	2	2217	16.80	8.09	0.48
	3	2195	16.60	7.99	0.48
	4	2504	18.97	9.06	0.48
	5	2153	16.30	11.14	0.68
	Average	2277	17.23	9.02	0.53
	Std. Dev.	140	1.07	1.27	0.09
0.4_3%MNPs_0T	1	3723	28.20	19.45	0.69
	2	4145	31.40	22.15	0.71
	3	4100	31.10	22.78	0.73
	4	4140	31.40	16.21	0.52
	5	6150	46.60	29.07	0.62
	6	3670	27.80	17.08	0.61
	7	5714	43.30	20.22	0.47
	8	7738	58.60	38.72	0.44
	Average	4923	37.30	23.21	0.60
	Std. Dev.	1462	11.07	7.42	0.11
0.4_3%MNPs_0.25 T	1	5223	39.60	32.09	0.81
	2	6511	49.30	33.79	0.69
	3	8135	61.60	42.62	0.69
	4	8169	61.90	46.56	0.75
	5	7151	54.20	39.27	0.73
	6	9751	73.90	58.54	0.79
	7	6620	50.20	29.67	0.59
	8	8727	66.10	44.67	0.68
	9	9057	68.10	46.43	0.68
	10	9548	72.30	70.41	0.97
	11	6968	52.80	27.74	0.53
	12	9750	73.90	56.56	0.77
	Average	7968	60.33	44.03	0.72
	Std. Dev.	1472	11.11	12.86	0.11
0.4_3%MNPs_0.5 T	1	20,400	154.50	198.56	1.29
	2	11,275	85.40	96.21	1.13
	3	8847	67.00	64.15	0.96
	4	10,361	78.50	100.30	1.28
	5	20,489	157.50	200.46	1.27
	6	6989	52.90	37.69	0.71
	7	5230	39.62	37.28	0.94
	8	9140	69.20	107.87	1.56
	9	12,504	94.70	119.91	1.27
	10	11,372	86.20	96.76	1.12
	Average	11,661	88.55	105.92	1.15
	Std. Dev.	5103	39.10	56.80	0.24
0.4_3%MNPs_0.75 T	1	11,911	90.20	119.19	1.32
	2	9484	71.80	83.22	1.16
	3	12,455	94.40	156.48	1.66
	4	12,088	91.60	135.79	1.48
	5	10,878	82.40	119.25	1.45
	6	9681	73.30	57.27	0.78
	7	8658	65.60	91.91	1.40
	8	6965	52.80	85.05	1.61
	9	12,332	93.40	119.63	1.28
	10	14,138	107.10	154.25	1.44

(*continued on next page*)

(*continued*)

Mixture	Image	N*	N_M	SD	COV
	11	12,097	91.60	115.93	1.27
	Average	10,972	83.11	112.54	1.35
	Std. Dev.	2068	15.66	30.75	0.24
0.4_1%MNPs_0T	1	2883	21.80	11.56	0.53
	2	3094	23.40	14.75	0.63
	3	4713	35.17	17.56	0.49
	4	3096	23.50	11.04	0.47
	Average	3447	25.97	13.73	0.53
	Std. Dev.	850	6.18	3.04	0.07
0.4_1%MNPs_0.5 T	1	3960	30.00	16.84	0.56
	2	5700	43.20	35.85	0.83
	3	3937	29.80	13.63	0.46
	4	3468	26.30	15.64	0.60
	5	4837	36.60	38.95	1.06
	6	5318	40.30	33.80	0.84
	Average	4537	34.37	25.79	0.72
	Std. Dev.	882	6.68	11.57	0.23
0.35_3%MNPs_0T	1	10,718	81.20	39.81	0.49
	2	8727	66.10	26.81	0.41
	3	9978	75.60	32.50	0.43
	4	8097	61.30	25.75	0.42
	5	9676	73.30	45.13	0.62
	6	9576	72.50	55.08	0.76
	7	15,566	117.90	118.97	1.01
	8	6228	47.20	24.29	0.52
	9	11,188	84.80	87.28	1.03
	10	10,387	78.70	74.91	0.95
	11	7627	57.80	28.36	0.49
	Average	9797	74.22	50.81	0.65
	Std. Dev.	2408	18.24	30.78	0.25
0.35_3%MNPs_0.5 T	1	6553	49.60	51.77	1.04
	2	8712	66.00	83.79	1.27
	4	4655	35.30	26.88	0.76
	5	8033	60.90	73.33	1.21
	6	10,203	77.30	113.61	1.47
	7	10,887	82.50	63.26	0.77
	8	9962	75.50	67.63	0.90
	Average	8429	63.87	68.61	1.06
	Std. Dev.	2219	16.81	26.87	0.27
0.35_0.6%PCE_3%MNPs_0T	1	3521	26.70	24.58	0.92
	2	8605	65.20	47.53	0.73
	3	9858	74.70	75.48	1.01
	4	5739	43.50	54.92	1.26
	5	2751	20.80	23.99	1.15
	6	8051	61.00	58.87	0.97
	7	5248	39.80	37.36	0.94
	8	4776	36.20	17.70	0.49
	9	3872	30.10	28.03	0.93
	10	2558	19.38	17.21	0.89
	Average	5498	41.74	38.57	0.93
	Std. Dev.	2551	19.28	19.82	0.21
0.35_0.6%PCE_3%MNPs_0.5 T	1	6267	47.48	55.23	1.16
	2	8605	65.20	47.53	0.73
	3	9858	74.70	75.48	1.01
	4	5736	43.50	54.92	1.26
	5	2751	20.80	23.99	1.15
	6	8051	61.00	58.87	0.97
	7	4725	35.80	32.26	0.90
	8	8066	61.11	77.37	1.27
	9	5132	38.88	37.53	0.97
	10	9160	69.40	60.38	0.87
	11	9107	68.99	95.78	1.39
	Average	7042	53.35	56.30	1.06
	Std. Dev.	2257	17.10	21.09	0.20

Appendix B. Representative figures of Fe-element quantitative distribution for each mixture

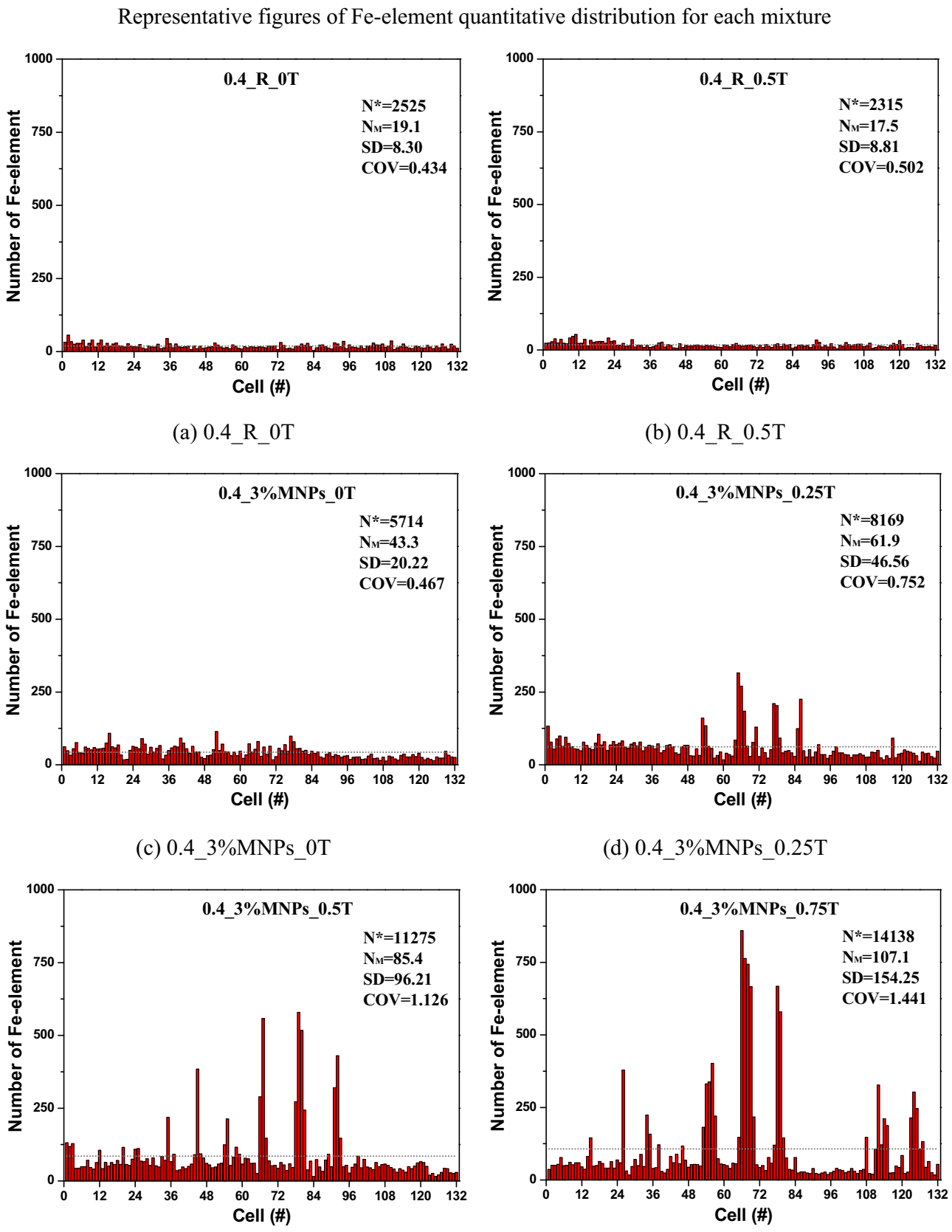

(a) 0.4_R_0T

(b) 0.4_R_0.5T

(c) 0.4_3%MNPs_0T

(d) 0.4_3%MNPs_0.25T

(e) 0.4_3%MNPs_0.5T

(f) 0.4_3%MNPs_0.75T

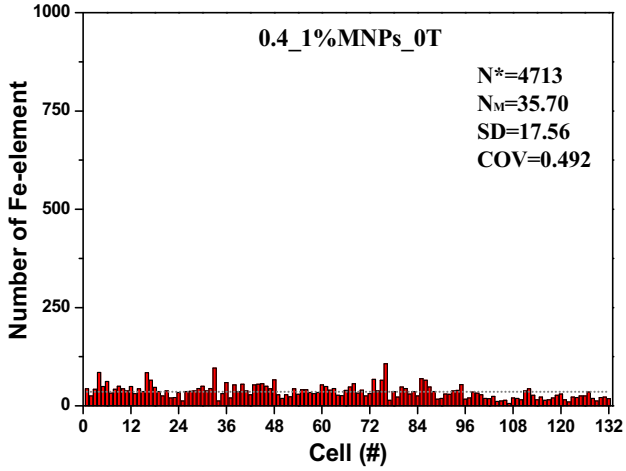

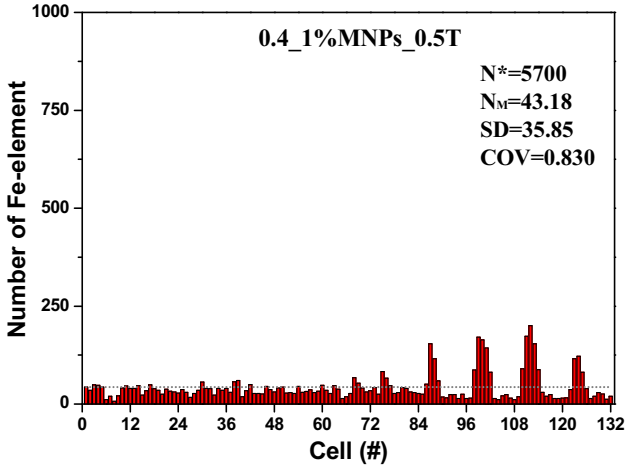

(g) 0.4_1%MNPs_0T

(h) 0.4_1%MNPs_0.5T

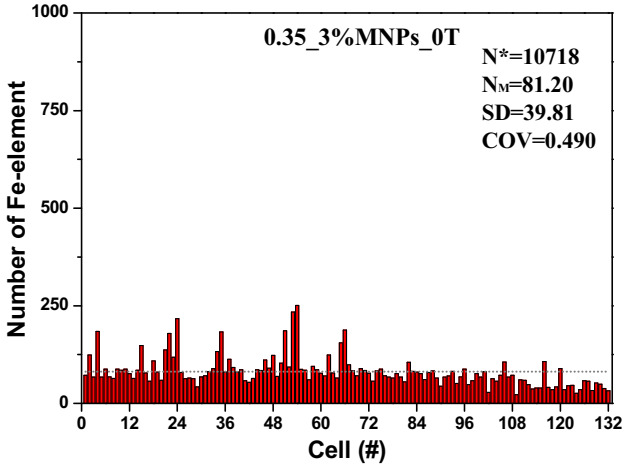

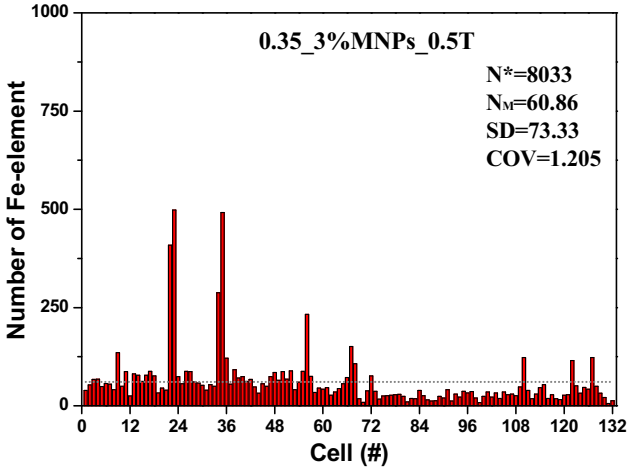

(i) 0.35_3%MNPs_0T

(j) 0.35_3%MNPs_0.5T

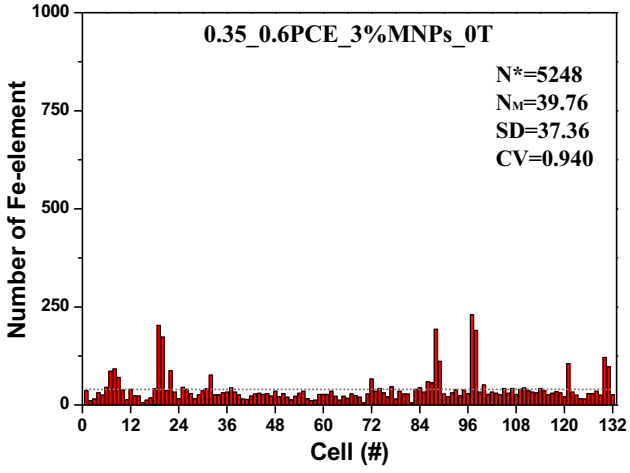

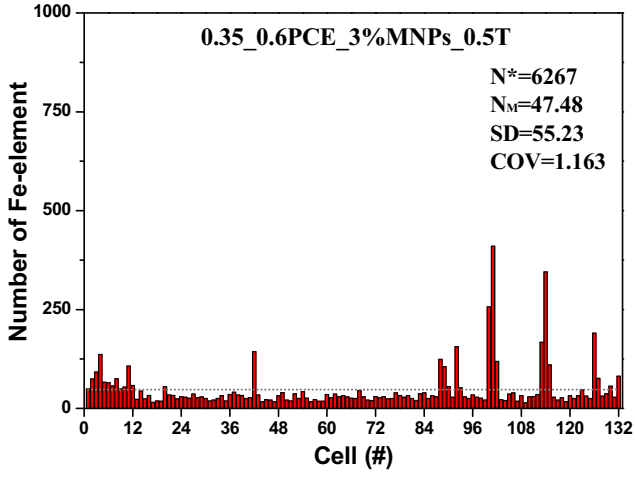

(k) 0.35_0.6%PCE_3%MNPs_0T

(l) 0.35_0.5%PCE_3%MNPs_0.5T

. (*continued*).

References

[1] G. De Schutter, D. Feys, Pumping of fresh concrete: insights and challenges, RILEM Technical Letters 1 (2016) 76–80.
[2] E. Secrieru, D. Cotardo, V. Mechtcherine, L. Lohaus, C. Schröfl, C. Begemann, Changes in concrete properties during pumping and formation of lubricating material under pressure, Cem. Concr. Res. 108 (2018) 129–139.
[3] G. De Schutter, Thixotropic Effects During Large-scale Concrete Pump Tests on Site, 71st RILEM Annual Week & ICACMS 2017Chennai, India, 2017.
[4] G. Ovarlez, N. Roussel, A physical model for the prediction of lateral stress exerted by self-compacting concrete on formwork, Mater. Struct. 39 (2006) 269–279.
[5] N. Roussel, A thixotropy model for fresh fluid concretes: theory, validation and applications, Cem. Concr. Res. 36 (2006) 1797–1806.
[6] N. Roussel, Rheology of fresh concrete: from measurements to predictions of casting processes, Mater. Struct. 40 (2007) 1001–1012.
[7] G. De Schutter, K. Lesage, V. Mechtcherine, V.N. Nerella, G. Habert, I. Agusti-Juan, Vision of 3D printing with concrete - technical, economic and environmental potentials, Cem. Concr. Res. 112 (2018) 25–36.
[8] Q. Yuan, Z. Li, D. Zhou, T. Huang, H. Huang, D. Jiao, C. Shi, A feasible method for measuring the buildability of fresh 3D printing mortar, Constr. Build. Mater. 227 (2019) 116600.
[9] G. De Schutter, K. Lesage, Active control of properties of concrete: a (p)review, Mater. Struct. 51 (2018) 123.
[10] W. Meng, K.H. Khayat, Improving flexural performance of ultra-high-performance concrete by rheology control of suspending mortar, Compos. Part B 117 (2017) 26–34.
[11] S.Z. Jones, D.P. Bentz, N.S. Martys, W.L. George, A. Thomas, Rheological control of 3D printable cement paste and mortars, Rilem Bookser 19 (2019) 70–80.
[12] D. Jiao, C. Shi, Q. Yuan, X. An, Y. Liu, H. Li, Effect of constituents on rheological properties of fresh concrete-a review, Cem. Concr. Compos. 83 (2017) 146–159.
[13] D. Jiao, C. Shi, Q. Yuan, X. An, Y. Liu, Mixture design of concrete using simplex centroid design method, Cem. Concr. Compos. 89 (2018) 76–88.
[14] D. Marchon, S. Kawashima, H. Bessaies-Bey, S. Mantellato, S. Ng, Hydration and rheology control of concrete for digital fabrication: potential admixtures and cement chemistry, Cem. Concr. Res. 112 (2018) 96–110.
[15] D. Jiao, K. El Cheikh, C. Shi, K. Lesage, G. De Schutter, Structural build-up of cementitious paste with nano-Fe3O4 under time-varying magnetic fields, Cem. Concr. Res. 124 (2019) 105857.
[16] S.D. Nair, R.D. Ferron, Set-on-demand concrete, Cem. Concr. Res. 57 (2014) 13–27.
[17] S.D. Nair, R.D. Ferron, Real time control of fresh cement paste stiffening: smart cement-based materials via a magnetorheological approach, Rheol. Acta 55 (2016) 571–579.
[18] E. Horszczaruk, Properties of cement-based composites modified with magnetite nanoparticles: a review, Materials (Basel) 12 (2019) 326.
[19] P. Sikora, E. Horszczaruk, K. Cendrowski, E. Mijowska, The influence of Nano-Fe3O4 on the microstructure and mechanical properties of Cementitious composites, Nanoscale Res. Lett. 11 (2016) 182.
[20] M.S. Amin, S.M.A. El-Gamal, F.S. Hashem, Effect of addition of nano-magnetite on the hydration characteristics of hardened Portland cement and high slag cement pastes, J. Therm. Anal. Calorim. 112 (2012) 1253–1259.
[21] M.O.G.P. Bragança, K.F. Portella, M.M. Bonato, E. Alberti, C.E.B. Marino, Performance of Portland cement concretes with 1% nano-Fe3O4 addition: electrochemical stability under chloride and sulfate environments, Constr. Build. Mater. 117 (2016) 152–162.
[22] I. Mansouri, M. Nejat, S. Shahbazi, A. Karami, Effect of magnetite nanoparticles (ferroferric oxide) on discrete concrete properties, Proceedings of the Institution of Civil Engineers-Construction Materials (2018) 1–8.
[23] Y. He, L. Lu, K. Sun, F. Wang, S. Hu, Electromagnetic wave absorbing cement-based composite using Nano-Fe3O4 magnetic fluid as absorber, Cem. Concr. Compos. 92 (2018) 1–6.
[24] R. Mu, H. Li, L. Qing, J. Lin, Q. Zhao, Aligning steel fibers in cement mortar using electro-magnetic field, Constr. Build. Mater. 131 (2017) 309–316.
[25] I. Abavisani, O. Rezaifar, A. Kheyroddin, Alternating magnetic field effect on fine-aggregate steel chip–reinforced concrete properties, J. Mater. Civ. Eng. 30 (2018), 04018087.
[26] M.S. Choi, Y.S. Kim, J.H. Kim, J.-S. Kim, S.H. Kwon, Effects of an externally imposed electromagnetic field on the formation of a lubrication layer in concrete pumping, Constr. Build. Mater. 61 (2014) 18–23.
[27] J.H. Park, B.D. Chin, O.O. Park, Rheological properties and stabilization of magnetorheological fluids in a water-in-oil emulsion, J. Colloid Interface Sci. 240 (2001) 349–354.
[28] N.M. Wereley, A. Chaudhuri, J.H. Yoo, S. John, S. Kotha, A. Suggs, R. Radhakrishnan, B.J. Love, T.S. Sudarshan, Bidisperse magnetorheological fluids using Fe particles at nanometer and Micron Scale, J. Intell. Mater. Syst. Struct. 17 (2006) 393–401.
[29] S. Vinod, R. John, J. Philip, Magnetorheological properties of sodium sulphonate capped electrolytic iron based MR fluid: a comparison with CI based MR fluid, Smart Mater. Struct. 26 (2017), 025003.
[30] B.S. En, Methods of testing cement—part 1: determination of strength, European Committee for Standardization: Brussels, Belgium 169 (2005) 36.
[31] Q. Song, R. Yu, Z. Shui, X. Wang, S. Rao, Z. Lin, Optimization of fibre orientation and distribution for a sustainable Ultra-High Performance Fibre Reinforced Concrete (UHPFRC): experiments and mechanism analysis, Constr. Build. Mater. 169 (2018) 8–19.
[32] P. Estelle, S. Halelfadl, N. Doner, T. Mare, Shear history effect on the viscosity of carbon nanotubes water-based nanofluid, Curr. Nanosci. 9 (2013) 225–230.
[33] D. Jiao, C. Shi, Q. Yuan, Time-dependent rheological behavior of cementitious paste under continuous shear mixing, Constr. Build. Mater. 226 (2019) 591–600.
[34] D. Jiao, K. El Cheikh, K. Lesage, C. Shi, G. De Schutter, Structural build-up of cementitious paste under external magnetic fields, rheology and processing of construction materials, Springer (2019) 36–42.
[35] D. Jiao, C. Shi, K. Lesage, K. El Cheikh, G. De Schutter, Effects of external magnetic field on structural evolution of cement paste with nano-Fe3O4, 2nd International Conference on UHPC Materials and Structures (UHPC2018-China), Fuzhou, China (2018) 344–348.
[36] D. Jiao, K. Lesage, M. Yucel Yardimci, K. El Cheikh, C. Shi, G. De Schutter, Rheological behavior of cement paste with nano-Fe3O4 under magnetic field: Theoretical derivations and magneto-rheological responses, Cement and Concrete Research, (2020) Under Review.
[37] A. Korpa, T. Kowald, R. Trettin, Hydration behaviour, structure and morphology of hydration phases in advanced cement-based systems containing micro and nanoscale pozzolanic additives, Cem. Concr. Res. 38 (2008) 955–962.
[38] D. Kong, Y. Su, X. Du, Y. Yang, S. Wei, S.P. Shah, Influence of nano-silica agglomeration on fresh properties of cement pastes, Constr. Build. Mater. 43 (2013) 557–562.